34th Annual International Conference of the IEEE EMBS
San Diego, California USA, 28 August - 1 September, 2012

Bivariate point process modeling and joint non-stationary analysis of pulse transit time and heart period

Michele Orini, Luca Citi*, *Member IEEE*, Riccardo Barbieri, *Senior Member IEEE*

***Abstract*— Pulse transit time (PTT) is strictly related to pulse wave velocity and may be used for non-invasive monitoring of arterial stiffness and pressure, whose assessment is fundamental to detect cardiovascular dysfunctions. We propose a new model to characterize instantaneous PTT dynamics, and the interactions between PTT and R-R interval (RRI). In this model, PTT is described as a point process whose probability function depends on previous PTT and RRI values. From the model coefficients, instantaneous powers, coherence and directed coherence of each spectral component are estimated. We used this framework to study the changes that tilt table test provoked in PTT and RRI dynamics in 17 healthy subjects. Time-varying spectral and coherence analysis revealed that, although PTT and RRI were locally correlated, direct contribution of RRI on PTT was low during the entire test in high frequency band, and just after postural changes in low frequency band. We conclude that PTT may add valuable information for a more accurate characterization of cardiovascular regulation.**

I. INTRODUCTION

Pulse transit time (PTT) is the time it takes a pulse wave to travel between two arterial sites [1], and it is often estimated as the time delay between the R-wave of the ECG (ventricular contraction) and the arrival time of the pulse wave to the finger. Pulse transit time is strictly related to pulse wave velocity [2]. Thus, an appropriate processing of PTT may offer the possibility of estimating, non-invasively, arterial blood pressure [2], [3] and arterial stiffness [4], whose assessment is fundamental to detect cardiovascular dysfunctions. This possibility is even more interesting considering that PTT can be estimated by just using ECG and pulse photoplethysmograph (PPG) devices [5], which are widely employed, cheap, and comfortable.

In this study, we propose to continuously estimate PTT by using a point process approach [6]. Being defined as a waiting time between two events, PTT can be considered as a point process triggered by the R-wave events, whose occurrence time is also a point process [6]. Therefore, we set up a bivariate model between PTT and R-R intervals (RRI) and we used it to describe the dynamic interactions between them. We assessed the capability of the model to capture the statistical dynamics of PTT during tilt table test, and we used time-varying parametric analysis to estimate the instantaneous powers of the signal spectral components, as well as coherence and directed coherence between them [7].

This work was supported in part by NIH grant R01-HL084502, and by Ministerio de Ciencia y Tecnología, FEDER under Project TEC2010-21703-C03-02, and TRA2009-0127, and by ARAID and Ibercaja under project Programa de apoyo a la I+D+i.

M. Orini is with GTC, I3A, IIS Aragón, Universidad de Zaragoza and with CIBER–BBN, Zaragoza, Spain; michele@unizar.es

L. Citi and R. Barbieri are with the Department of Anesthesia, Critical Care and Pain Medicine, MGH–Harvard Medical School, Boston, MA, USA, and with the Department of Brain and Cognitive Sciences, MIT, Cambridge, MA, USA. {lciti,barbieri}@neurostat.mit.edu

* Corresponding Author.

II. METHODS

A. The R-R interval as a point process

To statistically describe RRI dynamics, let's first define the time occurrence of the n-th R wave in the ECG as t_n^R and the n-th RRI as $w_n^{RR} = t_{n+1}^R - t_n^R$ (see Fig. 1). The probability density function of the duration of the RRI can be described for any $t > t_n^R$ by a history-dependent (HD) inverse Gaussian (IG) distribution [6]:

$$f_{RR}(t) = \sqrt{\frac{\lambda_{RR}(t)}{2\pi[t-t_n^R]^3}} \exp\left(-\frac{\lambda_{RR}(t)[t-t_n^R-\mu_{RR}(t)]^2}{2\mu_{RR}^2(t)[t-t_n^R]}\right) \quad (1)$$

where $\mu_{RR}(t)$ and $\lambda_{RR}(t)$ are the mean and the shape parameters, which completely define the distribution. The recent history of the RRI series affects the duration of any new RRI [6]. This dependency is introduced by modeling the mean of the IG as a linear function of P past w_n^{RR}:

$$\mu_{RR}(t) = a_0^{(11)}(t) + \sum_{k=1}^{P} a_k^{(11)}(t) w_{n-k}^{RR} \quad (2)$$

B. Bivariate point process to describe PTT dynamics

Pulse transit time can be seen as a point process, which in turn depends on a point process: the heart period. The n-th PTT is defined as $w_n^{PTT} = t_n^P - t_n^R$, where t_n^P is the occurrence time of the n-th pulse in the PPG signal (see Fig. 1). For $t_n^R < t < t_n^P$, the PTT is described by a HDIG distribution as:

$$f_{PTT}(t) = \sqrt{\frac{\lambda_{PTT}(t)}{2\pi[t-t_n^R]^3}} \exp\left(-\frac{\lambda_{PTT}(t)[t-t_n^R-\mu_{PTT}(t)]^2}{2\mu_{PTT}^2(t)[t-t_n^R]}\right) \quad (3)$$

where $\mu_{PTT}(t)$ and $\lambda_{PTT}(t)$ are the mean and the shape parameters of the IG. RRI and PTT are modeled as mutually interacting: past w_n^{RR} and w_n^{PTT} both affect $\mu_{RR}(t)$ and $\mu_{PTT}(t)$, the means of the $f_{RR}(t)$ and $f_{PTT}(t)$, respectively:

$$\mu_{RR}(t) = a_0^{(11)}(t) + \sum_{k=1}^{P} a_k^{(11)}(t) w_{n-k}^{RR} + \sum_{k=1}^{Q} a_k^{(12)}(t) w_{n-k}^{PTT} \quad (4)$$

$$\mu_{PTT}(t) = a_0^{(22)}(t) + \sum_{k=1}^{P} a_k^{(21)}(t) w_{n-k}^{RR} + \sum_{k=1}^{Q} a_k^{(22)}(t) w_{n-k}^{PTT} \quad (5)$$

These bivariate autoregressive equations are properly updated corresponding to the point process events t_n^R and t_n^P.

In expressions (4)–(5), $a_k^{(ij)}(t)$ are the model coefficients which continuously characterize the dynamic interactions between RRI and PTT. In particular, $a_k^{(11)}(t)$ and $a_k^{(22)}(t)$

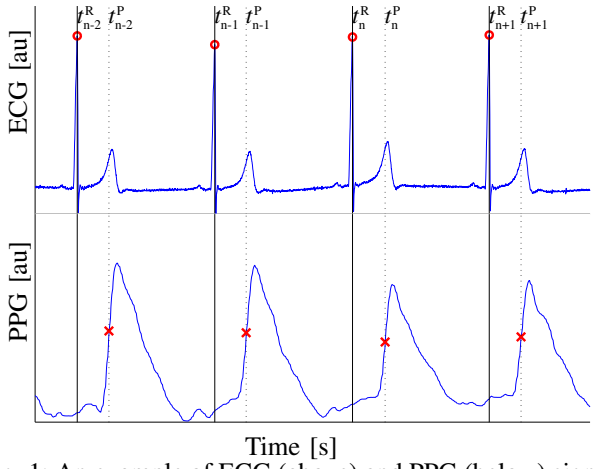

Fig. 1: An example of ECG (above) and PPG (below) signals. Circles and crosses mark the occurrence time of a R wave, t_n^R, and the reference t_n^P in the PPG signal used to estimate the PTT.

account for the pure autoregressive part of the model, $a_k^{(12)}(t)$ quantifies the linear contribution that the $(n-k)$-th PTT value has on $\mu_{RR}(t)$, while $a_k^{(21)}(t)$ quantifies the linear contribution that the $(n-k)$-th RR interval has on $\mu_{PTT}(t)$.
The standard deviations of the processes [6]:

$$\sigma_{RR} = \sqrt{\mu^3_{RR}(t)/\lambda_{RR}(t)};\ \sigma_{PTT} = \sqrt{\mu^3_{PTT}(t)/\lambda_{PTT}(t)} \quad (6)$$

are used as estimates of RRI and PTT variability, respectively. Time-varying model coefficients are identified by Newton-Raphson maximization of the local likelihood, which also includes right censoring, and using a waiting function $W(t-t_n^R) = 0.98^{(t-t_n^R)}$, with $t-t_n \leq 90$ s [6].
To assess the capability of the model to describe the statistical properties of both RRI and PTT series, the model goodness-of-fit is quantified. Goodness-of-fit is evaluated by representing the Kolmogorov-Smirnov (KS) plot which measures the largest distance between the cumulative distribution function of RRI and PTT series transformed to the interval (0,1] by using the time rescaling theorem [6], and the cumulative distribution function of a uniform distribution on (0,1]. The smaller the KS distances, the closer is the agreement between original RRI and PTT series and the proposed model. If the model completely captures the statistical properties of RRI and PTT, the transformed series should be also uncorrelated [6]. Thus, as further measure of goodness-of-fit, autocorrelations of the transformed series are also estimated. To quantify the degree of correlation in the rescaled series, two indices were estimated: the number of the lag points for which the correlation was outside the confidence interval, $c_\#$, and the ratio between the highest correlation and the confidence level, c_R.

C. Characterization of the dynamic interactions between PTT and RRI

1) Time-frequency representations: Once the model coefficients have been estimated, they can be used to characterize the dynamic interactions between RRI and PTT. Let's define:

$$\mathbf{A}_k(t) = \begin{bmatrix} a_k^{(11)}(t) & a_k^{(12)}(t) \\ a_k^{(21)}(t) & a_k^{(22)}(t) \end{bmatrix} \quad (7)$$

Coefficients are projected from the time-lag domain to the frequency domain by Fourier transform:

$$\mathbf{A}(t,f) = \sum_{k=1}^{M} \mathbf{A}_k(t) e^{-i2\pi fk} \quad \mathbf{H}(t,f) = [\mathbf{I} - \mathbf{A}(t,f)]^{-1} \quad (8)$$

where $\mathbf{H}(t,f)$ is the non-stationary transfer function of the system, and M is the order of the model $M = \max(P,Q)$. Spectra, $S_{ij}(t,f)$, coherence $\gamma_{ij}(t,f)$ and directed coherence $\gamma_{ij}^{DC}(t,f)$ are defined, for $\{i,j\} \in \{1,2\}$, as [7], [8]:

$$S_{ij}(t,f) = \sum_{m=1}^{2} H_{im}(t,f)\sigma_m^2(t)H_{jm}^*(t,f) \quad (9)$$

$$\gamma_{ij}(t,f) = \frac{S_{ij}(t,f)}{\sqrt{S_{ii}(t,f)S_{jj}(t,f)}} \quad (10)$$

$$\gamma_{ij}^{DC}(t,f) = \frac{\sigma_j(t)H_{ij}(t,f)}{\sqrt{\sigma_1^2(t)|H_{i1}(t,f)|^2 + \sigma_2^2(t)|H_{i2}(t,f)|^2}} \quad (11)$$

Coherence $|\gamma_{ij}(t,f)| = |\gamma_{ji}(t,f)|$ quantifies the strength of the linear local coupling between RRI and PTT, while $|\gamma_{ii}(t,f)| = |\gamma_{jj}(t,f)| = 1$. Directed coherence $\gamma_{ij}^{DC}(t,f)$ represents the ratio between the part of $S_{ii}(t,f)$ due to process j, and $S_{ii}(t,f)$ [7]. By definition, $|\gamma_{ii}^{DC}(t,f)|^2 + |\gamma_{ij}^{DC}(t,f)|^2 = 1$. Note also that in a bivariate model, $|\gamma_{ij}^{DC}(t,f)|$ is equal to the magnitude of the partial directed coherence evaluated along the same direction $j \to i$ [7].

2) Extraction of synchronization indices: To estimate the time course of the indices, a time-varying spectral band centered around $f_{ij,B}(t)$, the instantaneous frequency of the LF or HF spectral peak of $|S_{ij}(t,f)|$, is defined as: $\Omega_{ij,B} = \left\{(t,f) \in [\mathbb{R}^+ \times B] \middle| f = f_{ij,B}(t) \pm \frac{\Delta_F}{2}\right\}$, where $B \in \{LF, HF\}$ and $\Delta_F = 0.1$ Hz is the width of $\Omega_{ij,B}$. Note that $f_{ij,B}(t)$ is estimated only if a spectral peak is detected in $f \in B$. Moreover, $\Omega_{ij,LF}$ and $\Omega_{ij,HF}$ cannot overlap, and when respiratory rate decreases, $\Omega_{ij,HF}$ can include portion of the traditional LF band, LF$\in [0.04-0.15]$ Hz.
Instantaneous powers, $P_{i,B}(t)$, coherence, $\gamma_{ij,B}(t)$, and directed coherence, $\gamma_{ij,B}^{DC}(t)$, are estimated as:

$$P_{i,B}(t) = \frac{1}{\Delta_F}\int_{\Omega_{ij,B}} S_{ii}(t,f)df \quad (12)$$

$$\gamma_{ij,B}(t) = \max_{f=\Omega_{ij,B}} \gamma_{ij}(t,f);\quad \gamma_{ij,B}^{DC}(t) = \max_{f=\Omega_{ij,B}} \gamma_{ij}^{DC}(t,f) \quad (13)$$

III. MATERIALS

Seventeen volunteers (aged 28.5± 2.8 years, 11 males) without any previous cardiovascular history underwent a head up tilt table test according to the following protocol: 4 minutes in early supine position (T_{ES}), 5 minutes tilted head up to an angle of 70 degrees (T_{HT}) and 4 minutes back to later supine position (T_{LS}) [9], [10]. The PPG signal was recorded from index finger with a sampling frequency of 250 Hz, whereas standard lead V4 ECG signal was recorded with a sampling frequency of 1000 Hz. The temporal location of

each R wave in the ECG, t_n^R, was automatically determined using the algorithm described in [11] (see Fig. 1). The PPG signal was interpolated using cubic splines increasing the resolution in time up to an equivalent sampling rate of 1000 Hz. Each pulse wave in the PPG was detected as the maximum of the PPG signal within the interval $[t_n^R$+150 ms, $t_{n+1}^R]$. The PTT is estimated as the time going from the occurrence of a R wave, t_n^R, and the 50% peak value of the PPG wave, t_n^P [12] (see Fig. 1). Heart beat and pulse wave detections were manually supervised.

IV. RESULTS

A. The bivariate point process model

To determine the model order, we discretized the order selection $\{P,Q\} \in \{2,\ldots,11\}$, and we estimated the KS distances and the autocorrelations of the rescaled series [6]. We empirically found that $P = Q = 6$ was a good compromise between spectral resolution and goodness-of-fit. The temporal resolution, i.e. the sampling rate at which (1)-(5) were updated, was set at 0.001 s. The mean and the standard deviation of the HDIG distributions of a representative subject are shown in Fig. 2(a)-(b). Here postural changes provoked different and fast variations in $\mu_{RR}(t)$ and $\mu_{PTT}(t)$. Interestingly, the variability of both signals, quantified by $\sigma_{RR}(t)$ and $\sigma_{PTT}(t)$, changed in a similar way.

The goodness-of-fit was evaluated by means of both KS plot and autocorrelation of the rescaled RRI and PTT series. Figure 2(c) shows that the HDIG distributions provided a good fit: KS plot was inside the confidence interval for most of the quantiles, being the KS distance 0.043 and 0.057 for RRI and PTT, respectively. Figure 2(d) shows that the autocorrelation of the RRI rescaled series was always inside the 95% confidence interval, while that of the PTT rescaled series was slighly outside confidence interval for lag 1 and 7. For this subject $\{c_\#^{PTT}, c_\#^{RR}\} = \{2,0\}$ and $\{c_R^{PTT}, c_R^R\} = \{1.65, 0.66\}$ (see Sec. II-B). As reported in Table I, the analysis of the entire data-set gave similar results: KS distance were 0.078±0.016 and 0.046±0.016 for PTT and RRI, respectively, while $\{c_\#^{PTT}, c_\#^{RR}\} = \{2.35 \pm 2.02, 1.47 \pm 1.62\}$ and $\{c_R^{PTT}, c_R^{RR}\} = \{1.29 \pm 0.34, 1.29 \pm 0.45\}$.

B. Interactions between RRI and PTT

The model coefficients were used to explore the dynamic interactions between RRI and PTT along the entire tilt table test. Figure 3 shows the median time course of the indices defined in (12)–(13), estimated across the 17 subjects, while numerical results are reported in Table I. During head-up tilt, LF powers increased in both RRI and PTT, while HF powers decreased in RRI and increased in PTT (Fig. 3(a)–(b)). Coherence in LF decreased at the beginning of head-up tilt, and slowly increased afterwards (Fig. 3(c)). Coherence in HF decreased just after postural changes (Fig. 3(d)), and it was generally higher than in LF band. The time course of directed coherence, shown in Fig. 3(e)-(f), shows that in LF, RRI gave a substantial contribution on PTT oscillations, while PTT scarcely affected RRI. Interestingly, after the postural changes, $\gamma_{21,LF}^{DC}(t)$ decreased, suggesting that

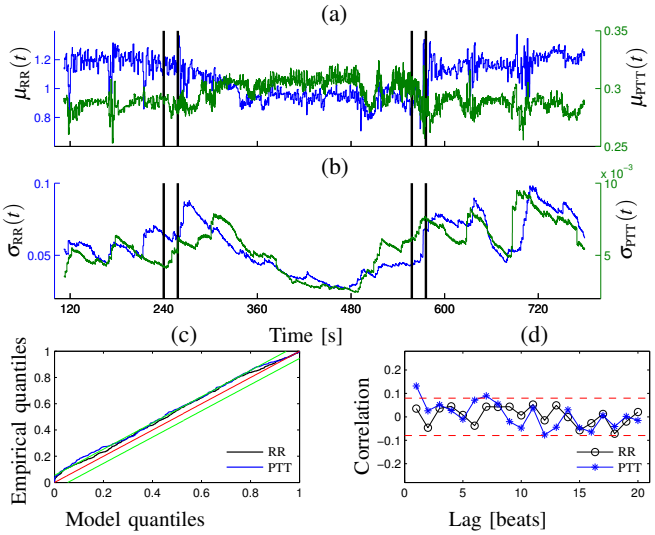

Fig. 2: (a)-(b) Mean and standard deviation of $f_{RR}(t)$ and $f_{PTT}(t)$ from a representative subject. Vertical lines separate T_{ES}, T_{HT} and T_{LS}. (c) KS plot of time rescaled series. (d) Autocorrelation functions of time rescaled series.

TABLE I: Goodness of fit: results are given as mean ± standard deviation of KS distances, $c_\#$ and c_R. PTT-RRI interactions: results are given as median / interquartile range, estimated across subjects, of temporal median of each index, estimated in each epoch.

Model goodness-of-fit			
Signal	KS-dist	$c_\#$	c_R
PTT	0.078±0.016	2.353±2.029	1.288±0.339
RRI	0.046±0.016	1.471±1.625	1.289±0.450

Indices of PTT-RRI interactions				
Index		T_{ES}	T_{HT}	T_{LS}
P_{LF}^{RR}	[e-03]	5.22 / 8.58	5.82 / 8.96	6.26 / 8.75
P_{HF}^{RR}	[e-03]	6.63 / 12.2	3.22 / 15.9	5.29 / 11.1
P_{LF}^{PTT}	[e-05]	3.24 / 4.17	8.86 / 13.2	3.57 / 4.18
P_{HF}^{PTT}	[e-05]	5.29 / 4.14	14.1 / 26.1	6.44 / 5.79
$\gamma_{12,LF}$	[nu]	0.927 / 0.139	0.818 / 0.192	0.878 / 0.196
$\gamma_{12,HF}$	[nu]	0.972 / 0.037	0.912 / 0.116	0.934 / 0.067
$\gamma_{12,LF}^{DC}$	[nu]	0.486 / 0.238	0.458 / 0.308	0.403 / 0.236
$\gamma_{12,HF}^{DC}$	[nu]	0.635 / 0.282	0.684 / 0.343	0.507 / 0.319
$\gamma_{21,LF}^{DC}$	[nu]	0.789 / 0.165	0.697 / 0.189	0.696 / 0.256
$\gamma_{21,HF}^{DC}$	[nu]	0.737 / 0.193	0.640 / 0.214	0.694 / 0.259

LF oscillations in PTT were less affected by RRI variability. In HF, the contribution of RRI variability on PTT was lower than in LF and it further decreased during head-up tilt. In T_{HT}, $\gamma_{12,HF}^{DC}(t) > \gamma_{21,HF}^{DC}(t)$, suggesting that orthostatic stress induced a change in the interactions between PTT and RRI around respiratory frequency. These changes may be related to previously documented changes observed during head-up tilt, suggesting a modification in the phase relationship between RRI and systolic blood pressure [13], and a different respiratory influence (in HF) on the pulse rate as compared to RR respiratory sinus arrhythmia [9].

V. DISCUSSION AND CONCLUSION

In this paper, we propose a model to characterize PTT dynamics and its interactions with the ECG-derived heart

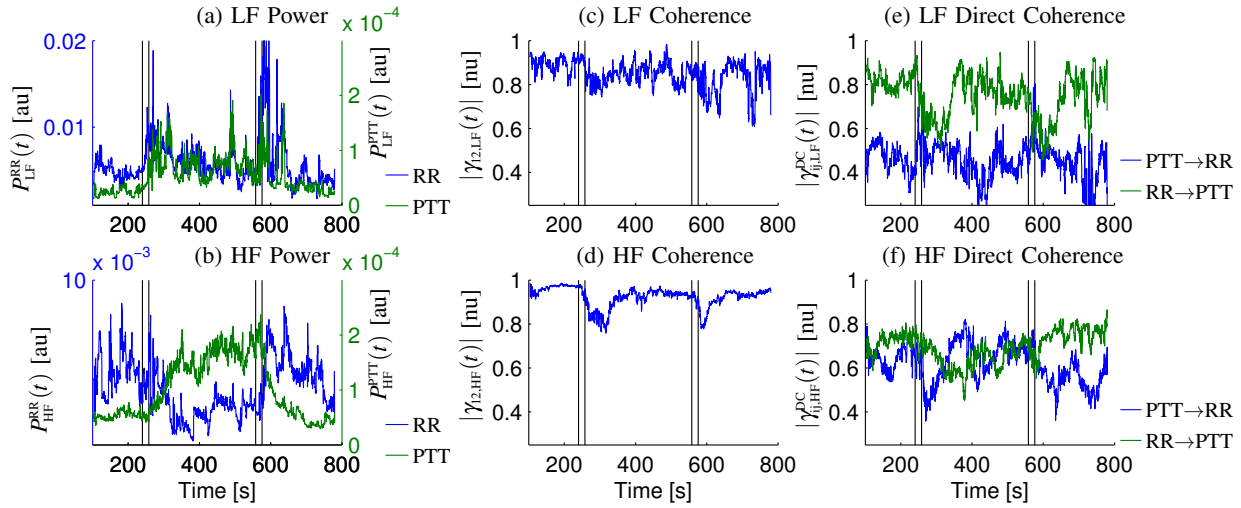

Fig. 3: Median time courses of indices characterizing PTT-RRI variability interactions, estimated across subjects. Vertical lines separate intervals of early supine position T_{ES}, head-up tilt T_{HT} and later supine position T_{LS}. Upper and lower graphics refer to results obtained in LF and HF bands, respectively. (a)-(b) Instantaneous powers $P_{i,B}(t)$; (c)-(d) Coherence $|\gamma_{12,B}(t)|$; (e)-(f) Directed coherence $|\gamma^{DC}_{12,B}(t)|$ and $|\gamma^{DC}_{21,B}(t)|$ are reported in blue and green line, respectively.

period. In the model, PTT is described as a point process characterized by a HDIG probability function, whose shape depends on previous PTT and RRI values. The combination of the point process approach and an autoregressive bivariate model allows to estimate the signal statistical properties and their interactions in continuous time [6], [8], respecting the precise chronological occurrence of each event. The local likelihood identification provided a satisfactory model goodness-of-fit. The strength of the coupling, and the contributions of RRI on PTT, were quantified by coherence and directed coherence, respectively [7].

We used this model to characterize the response of PTT to a tilt table test. We observed that passive postural changes provoked fast variations in the PTT. Although coherence analysis shows that PTT was locally linearly related to RRI, from directed coherence estimates we observed that PTT did not just depend on RRI, especially in HF band and in LF band after postural changes. This implies that PTT may add valuable information for a more accurate characterization of the cardiovascular regulation and the dynamic interactions between cardiovascular signals. The introduction of the PTT among the cardiovascular variables of interest introduces an important dimensionality associated to vascular regulation and its dynamics in the context of the entire cardiovascular control system.

REFERENCES

[1] J. E. Naschitz, S. Bezobchuk, R. Mussafia-Priselac, S. Sundick, D. Dreyfuss, I. Khorshidi, A. Karidis, H. Manor, M. Nagar, E. R. Peck, S. Peck, S. Storch, I. Rosner, and L. Gaitini, "Pulse transit time by r-wave-gated infrared photoplethysmography: review of the literature and personal experience." *J Clin Monit Comput*, vol. 18, no. 5-6, pp. 333–342, Dec 2004.

[2] W. Chen, T. Kobayashi, S. Ichikawa, Y. Takeuchi, and T. Togawa, "Continuous estimation of systolic blood pressure using the pulse arrival time and intermittent calibration," *Medical and Biological Engineering and Computing*, vol. 38, pp. 569–574, 2000.

[3] A. Porta, C. Gasperi, G. Nollo, D. Lucini, P. Pizzinelli, R. Antolini, and M. Pagani, "Global versus local linear beat-to-beat analysis of the relationship between arterial pressure and pulse transit time during dynamic exercise," *Medical and Biological Engineering and Computing*, vol. 44, no. 4, pp. 331–337, 2006.

[4] B. Pannier, A. Avolio, A. Hoeks, G. Mancia, and K. Takazawa, "Methods and devices for measuring arterial compliance in humans," *American Journal of Hypertension*, vol. 15, no. 8, pp. 743–753, 2002.

[5] J. Allen, "Photoplethysmography and its application in clinical physiological measurement." *Physiol Meas*, vol. 28, no. 3, pp. R1–39, Mar 2007.

[6] R. Barbieri, E. C. Matten, A. A. Alabi, and E. N. Brown, "A point-process model of human heartbeat intervals: new definitions of heart rate and heart rate variability," *American Journal of Physiology - Heart and Circulatory Physiology*, vol. 288, no. 1, pp. H424–H435, 2005.

[7] L. Faes and G. Nollo, *Biomedical Engineering, Trends in Electronics, Communications and Software*, 2011, ch. Multivariate Frequency Domain Analysis of Causal Interactions in Physiological Time Series.

[8] R. Barbieri, A. Bianchi, J. Triedman, L. Mainardi, S. Cerutti, and J. Saul, "Model dependency of multivariate autoregressive spectral analysis," *IEEE Eng. Med. Biol. Mag.*, vol. 16, no. 5, pp. 74–85, 1997.

[9] E. Gil, M. Orini, R. Bailón, J. M. Vergara, L. Mainardi, and P. Laguna, "Photoplethysmography pulse rate variability as a surrogate measurement of heart rate variability during non-stationary conditions," *Physiol Meas*, vol. 31, no. 9, p. 1271, 2010.

[10] A. Mincholé, E. Pueyo, J. F. Rodrguez, E. Zacur, M. Doblaré, and P. Laguna, "Quantification of restitution dispersion from the dynamic changes of the T-wave peak to end, measured at the surface ECG." *IEEE Trans Biomed Eng*, vol. 58, no. 5, pp. 1172–1182, May 2011.

[11] J. P. Martinez, R. Almeida, S. Olmos, A. P. Rocha, and P. Laguna, "A wavelet-based ECG delineator: Evaluation on standard databases," *IEEE Trans. Biomed. Eng.*, vol. 51, no. 4, pp. 570–581, 2004.

[12] E. Gil, R. Bailón, J. M. Vergara, and P. Laguna, "PTT variability for discrimination of sleep apnea related decreases in the amplitude fluctuations of PPG signal in children." *IEEE Trans Biomed Eng*, vol. 57, no. 5, pp. 1079–1088, May 2010.

[13] M. Orini, P. Laguna, L. T. Mainardi, and R. Bailón, "Assessment of the dynamic interactions between heart rate and arterial pressure by the cross time-frequency analysis." *Physiol Meas*, vol. 33, no. 3, pp. 315–331, Mar 2012.